06

# Electropulse ("sparking") plasma sintering of fine-grained W + 10 %Ni tungsten alloys

© E.A. Lantsev,<sup>1</sup> N.V. Malekhonova,<sup>1</sup> A.V. Nokhrin,<sup>1</sup> K.E. Smetanina,<sup>1</sup> A.A. Murashov,<sup>1</sup> A.V. Voronin,<sup>1</sup> Yu.V. Blagoveshchenskii,<sup>2</sup> A.V. Terent'ev<sup>2</sup>

<sup>1</sup>Lobachevsky University of Nizhny Novgorod, Nizhny,

603022 Novgorod, Russia <sup>2</sup>RAS Insitute of Metallurgy and Materials Science named after A.A. Baikov,

119334 Moscow, Russia

e-mail: elancev@nifti.unn.ru, malekhonova@nifti.unn.ru, yuriblag@imet.ac.ru

Received May 11, 2024 Revised December 23, 2024 Accepted March 10, 2025

The paper has investigated mechanisms of solid-phase electropulse plasma sintering of the  $W+10\,\mathrm{weight}\%\mathrm{Ni}$  tungsten pseudoalloy. The composite powders " W nucleus– Ni shell" were produced by a chemical-metallurgical method of deposition of nickel from a salt solution to a surface of industrial submicron tungsten particles. In order to reduce the oxygen and oxides concentrations, the composite powders were annealed in hydrogen at the temperatures  $400\,^\circ\mathrm{C}-600\,^\circ\mathrm{C}$ . It also included the X-ray studies of the phase composition, electron-microscopic studies of micro-structure parameters and measurement of hardness of the tungsten pseudoalloys. Using the Yang-Cutler model, diffusion mechanisms were defined, which determine kinetics of plasma sintering of the submicron powders " W nucleus– Ni shell". It has been shown that energy of powder sintering activation corresponds to energy of activation of diffusion along the grain boundaries in nickel, whereas a key mechanism of powder compaction is Coble creep.

Keywords: tungsten, electropulse plasma sintering, diffusion, hardness.

DOI: 10.61011/TP.2025.07.61455.150-24

### Introduction

The coarse-grained W–Ni tungsten pseudoalloys are composite materials, in which the solid particles  $\alpha$ -W are surrounded by the viscous  $\gamma$ -phase — the solid solution of tungsten in nickel [1–5]. The ultimate strength of the coarse-grained tungsten pseudoalloys produced by liquid phase sintering can be up to  $800-900\,\mathrm{MPa}$ , the Vickers hardness —  $2.5-3\,\mathrm{GPa}$ , while the ultimate elongation can exceed  $20\,\%-25\,\%$  [6,7]. This interesting and practically important combination of strength and plasticity in the coarse-grained tungsten pseudoalloys is due, first of all, to a composition and a structure of W/Ni interphase boundaries which form an almost continuous (closed) system across the material volume [1,5,8–10].

Presently, the researchers study applicability of the tungsten pseudoalloys with low content of the low-melting metal phase (below 10 weight%) for manufacturing heat, radiation- and plasma-resistant elements of structures of International Thermonuclear Experimental Reactor (ITER) (see, for example, [11-13]). It is assumed that adding a more plastic metal with the low neutron capture radius into tungsten facilitates to improve cracking resistance when fuel assemblies are affected by plasma pulses. In particular, it is shown in the study [14] that the Ni and Fe additives in the amount 3%-5% contribute to improvement of tungsten resistance to impact by powerful pulses of deuterium plasma. The papers [15,16] have also

demonstrated that a structure-phase state of the interphase boundaries is important for ensuring high resistance of tungsten pseudoalloys to plasma impact. In this regard, in recent years, there is an avalanche-like increase of the papers dedicated to a problem of creating the radiation- and plasma-resistance tungsten pseudoalloys for thermonuclear power engineering.

One of the effective methods of improving the physicalchemical properties of the tungsten pseudoalloys is to form a highly-dense ultra-fine-grained (UFG) microstructure [17-19] as well as to create in the material a high portion of "viscous" interphase W/Ni boundaries and, correspondingly, a minimum portion of the "brittle" W/W grain boundaries. In case of low-temperature solid-phase sintering of the powder compositions produced by mixing the W and Ni powders, it is difficult to ensure uniform distribution of nickel around the tungsten particles. It results in a big number of the W/W grain boundaries, which in case of lowtemperature sintering have low strength and in mechanical tests they can be nuclei of brittle microcracks [5,8,20]. Let us note that liquid phase sintering allows forming a system of continuous interphase boundaries in the tungsten pseudoalloys and it results in intense migration of the grain boundaries and, as a consequence, material softening.

A new promising approach to producing the UFG tungsten pseudoalloys with a large volume portion of the interphase boundaries is joint application of a technology of producing nano-composite particles by deposition of

fine metal layers to a surface of the submicron tungsten particles and a technology of their electropulse plasma sintering (EPPS). Let us note that technologies of synthesis of the composite particles with the structure "W nucleus—Ni shell" (that are being actively developed) (hereinafter referred to as W@Ni) [21,22] make it possible to use methods of low-temperature solid-phase sintering and to produce the tungsten pseudoalloys with high extension of the viscous W/Ni interphase boundaries. The study [22] (the year of 2021) was the first to report high mechanical properties of the W—Ni—Fe tungsten pseudoalloy produced by liquid phase sintering of the W@NiFe powders that are produced by electrodeposition. Later, the electrodeposition method was used to produce the composite powders W@Cu [23].

In comparison with traditional methods of mixing and high-energy powder grinding [24,25], an important advantage of the chemical metallurgy method of production of the W@Ni particles is that it is possible to avoid substantial pollution of the powders with grinding products (materials of mill hardware and grinding bodies), to avoid non-uniform distribution of the low-melting metal phase in the powder pressing volume, that can result in a higher portion of the W/W grain boundaries [26] as well as to minimize a poorly-controlled process of agglomeration of nano-powders, which substantially complicates the process of their sintering.

EPPS of the composite particles is carried out by passing a sequence of millisecond current high-power pulses through a graphite press form with the powder inside in conditions of pressure application [27]. Sintering can be carried out in vacuum or in a protective atmosphere. The EPPS technology based on the "sinter faster than the grain growth" principle makes it possible to produce the UFG samples with high strength and hardness [27–29].

The efficiency of joint application of these two methods has been previously exemplified by solving a task of producing UFG super-low-cobalt hard alloys [30,31]. Let us note that the EPPS can include local melting of the metal phase in an area of powder contact [32], thereby facilitating uniformity of nickle distribution throughout the volume of the tungsten pseudoalloy and contributing to formation of the "viscous" W/Ni interphase boundaries. This factor is very important in case of sintering at low temperatures, as the EPPS-produced tungsten pseudoalloys are characterized by a higher portion of the brittle W/W boundaries and, as a consequence, low plasticity [33]. Another factor facilitating formation the W/Ni interphase boundaries can be an effect of pseudo-incomplete wetting tungsten grain boundaries by nickel [34], which can be realized in conditions of solid-phase sintering of the W@Ni powders. In perspective, it will allow going to solving a crucial problem of creating the tungsten pseudoalloys with extremely low concentration of nickel, which have higher strength and plasticity (see [35,36]).

The present study is aimed at investigating the microstructure of the  $W+10\,\%\text{Ni}$  tungsten pseudoalloys produced by EPPS of the W@Ni composite powders.

# 1. Equipment, materials and methods of the experiment

The object of the study was the W + 10 weight%Ni tungsten pseudoalloys with the theoretical density  $\rho_{th}=17.24\,\mathrm{g/cm^3}$ . Initial materials were submicron industrial  $\alpha$ -W powders with the particle size of  $0.8\,\mu\mathrm{m}$  that are produced by Kirovgrad Solid Alloys Plant (KSAP). The concentration of oxygen in the  $\alpha$ -W powders was  $0.65\,\mathrm{weight\%}$ .

The  $\alpha$ -W powder was poured into a glass containing the alcohol solution NiCl<sub>2</sub> · 6H<sub>2</sub>O and the obtained mixture was heated to the temperature of 150 °C and held at this temperature with constant stirring so long as to produce a dry residue. The produced powders were annealed in the tube furnace Nabertherm RHTC 80-230/15 in accordance with the mode: heating to the temperature of 350 °C with holding for 30 min, then heating to  $T_{\rm H2} = 400\,^{\circ}\text{C}$ ,  $500\,^{\circ}\text{C}$ ,  $600\,^{\circ}\text{C}$ ,  $750\,^{\circ}\text{C}$  with holding at  $T_{\rm H2}$  for 3 h, and then — cooling with the furnace in an argon flow. In order to more effectively remove agglomerates, the W@Ni powders were wetly ground in the planetary mill Fritsch Pulverisette 16 and then dried in vacuum in the furnace Binder. The synthesis resulted in producing the W@Ni powders which were later used to sinter the tungsten pseudoal-

Prior to EPPS, the W@Ni powders were coldly pressed into cylindrical samples of the diameter of 12 mm and the height of 5 mm. They were pressed in steel press forms using a 10-t Sorokin press. For EPPS, the press forms made of high-strength MPG-7 graphite were used. In order to compensate thermal expansion of the samples and to increase closeness of their adjacency to the internal surface of the graphite press form, the samples were wrapped in a thin graphite sheet. Additionally, the graphite is designed to reduce the number of oxides on the surface of the metal particles [37]. The method of EPPS of the W-Ni tungsten pseudoalloys is described in detail in the paper [29] and we will not describe it in detail in order to The tungsten pseudoalloys have been manufactured using the installation "Dr. Sinter model SPS-625" (NJS Co., Japan). The electropulse sintering of the tungsten pseudoalloys: heating at the rate  $V_{h(1)} = 100 \,^{\circ}\text{C/min}$  to the temperature 600 °C, and then heating at the rate  $V_{h(2)} = 50$  °C/min to the temperature  $T_s$ , which corresponds to finishing of shrinkage (L) of the W@Ni powders. The time of isothermal holding of the W@Ni at the temperature  $T_s$  varied from 0 to 20 min. The EPPS of the samples was in the conditions of application of single-axis pressure (70 MPa), which remained constant  $(\pm 2 \,\mathrm{MPa})$  for the entire process of sample manufacturing. In order to remove graphite residues, after EPPS the surface of the samples of the tungsten pseudoalloys was cleaned by hydroabrasive treatement and subjected to mechanical grinding in order to remove a carbonized layer, which appears as a result of interaction of the material

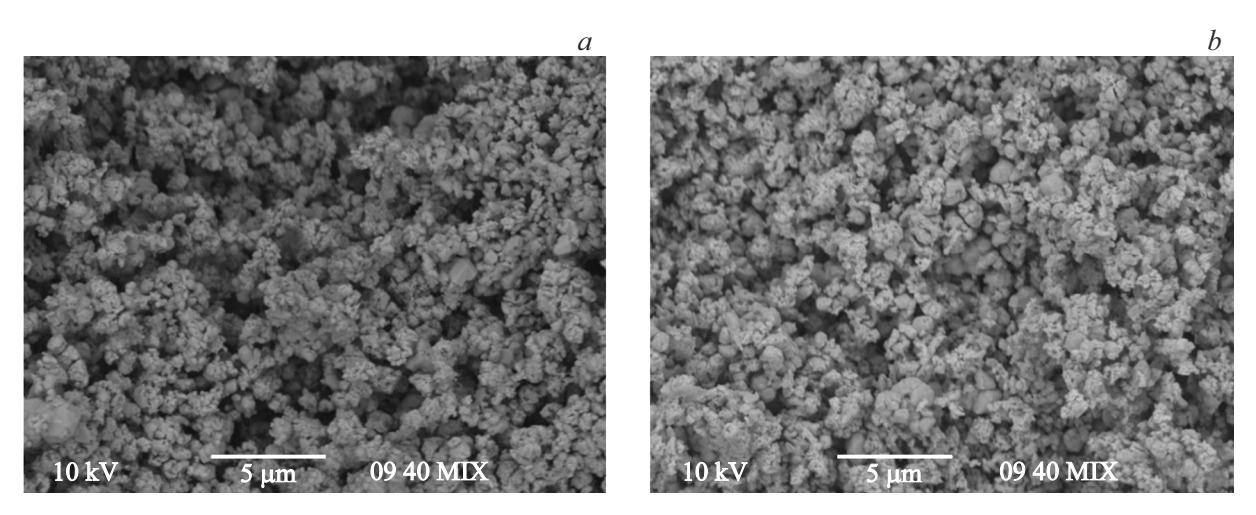


**Figure 1.** SEM images of the W@Ni powders annealed at  $T_{\rm H2} = 400\,^{\circ}{\rm C}$  (a) and  $600\,^{\circ}{\rm C}$  (b).

with the graphite press form [38] (in order to avoid the embrittlement effect that causes segregation of carbon and oxygen on the interphase boundaries of the tungsten pseudoalloy [39]).

The methods of investigation of the tungsten pseudoalloys are described in the study [29]. The density of the samples  $(\rho)$  was measured by hydrostatic weighing, while the microstructure of the tungsten pseudoalloys was studied by scanning electron microscopy (SEM). A phase composition of the powders and the alloys was investigated using the X-ray diffractometer DX-2700BH. Microhardness (HV) of the tungsten pseudoalloys was measured using the hardness tester Qness A60+.

## 2. Description of the experimental results

Fig. 1 shows electron-microscope images of the W@Ni particles that are produced by the chemical metallurgy

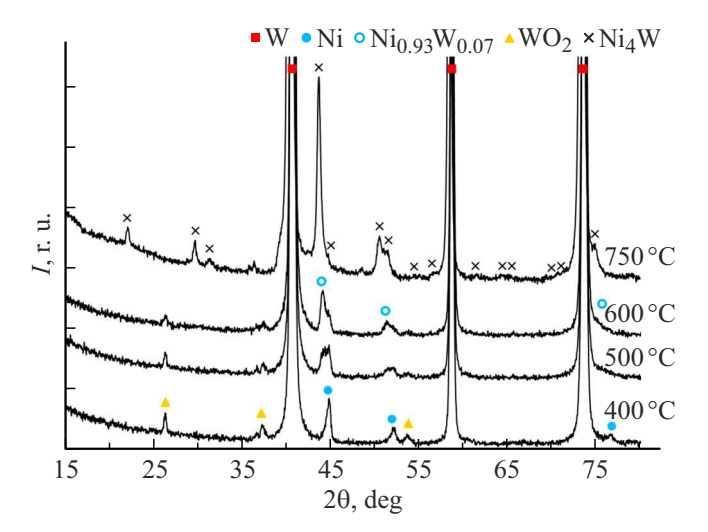


**Figure 2.** Diffraction patterns of the W@Ni powders after annealing in hydrogen at the various temperatures  $T_{\rm H2}$ .

method. The powders are of a submicron size and there are almost no large agglomerates inside the powder compositions. No trace of ground foreign impurities is found in the powders.

The diffraction patterns of Fig. 2 have been analyzed to show that the W@Ni powders contain the phases W (PDF № 00-004-0806, ICSD № 76151), Ni (PDF № 00-004-0850, ICSD  $N_0$  646089) and the impurity phase WO<sub>2</sub> (PDF  $N_{\odot}$  04-003-5856). The intensity of maxima attributed to the phase WO<sub>2</sub> decreases with increase of the temperature of hydrogen annealing. It is noted that with increase of the temperature of hydrogen annealing to 500 °C there is strong distortion of the crystal lattice of nickel, which indicates a beginning of intense dissolution of tungsten in Ni. This nickel-based y-phase can be identified as Ni<sub>0.93</sub>W<sub>0.07</sub> with the increased crystal lattice parameter [40]. The diffraction patterns of the powders annealed at 750°C have peaks of α-W and the intermetallic compound Ni<sub>4</sub>W (PDF № 96-152-3561). No other phase including Ni is detected in the powders. Therefore, nickel reacted with tungsten to produce the phase of the intermetallic compound Ni<sub>4</sub>W. In this regard, the further experiments were conducted with the powders annealed at 400 °C-600 °C.

Fig. 3 shows the temperature dependences of shrinkage L(T) and the shrinkage rate S(T) for the W@Ni powders annealed in hydrogen at the different temperatures. For convenience of analysis, the curves L(T) and S(T) have no portion of isothermal holding. The dependences L(T) are of a classic three-stage nature. It is clear from the graphs L(T) of Fig. 3, a that increase of  $T_{\rm H2}$  results in insignificant reduction of shrinkage and the shrinkage rate of the powders. Intense shrinkage of the composite W@Ni powders is finished at the temperature  $980\,^{\circ}{\rm C}{-}1000\,^{\circ}{\rm C}$ , while the maximum shrinkage rate  $(S_{\rm max} = (1.7{-}1.8) \cdot 10^{-2}\,{\rm mm/s})$  is achieved at  $840\,^{\circ}{\rm C}{-}850\,^{\circ}{\rm C}$ .

The density of the tungsten pseudoalloys sintered by heating to the temperature  $1050 \,^{\circ}\text{C}$  without isothermal holding ( $t_{\text{SPS}} = 0 \,\text{min}$ ) is  $17.075 \,\text{g/cm}^3$  (99.04%),  $17.243 \,\text{g/cm}^3$ 

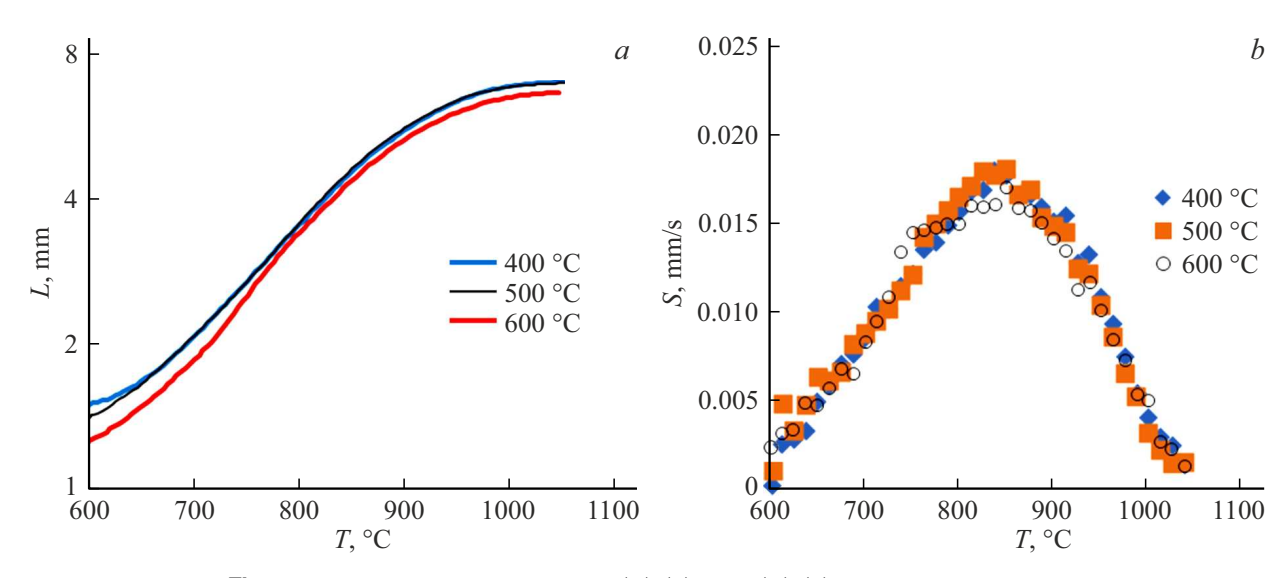


**Figure 3.** Temperature dependences L(T) (a) and S(T) (b) of the W@Ni powders.

(100.02%) and 17.211 g/cm³ (99.83%) for the powders annealed at 400 °C, 500 °C, 600 °C, respectively. Increase of the time of isothermal holding to 20 min at the sintering temperature (1050 °C) results in increase of the density of the pseudoalloys sintered from the powders annealed at 400 °C, 500 °C, 600 °C to 17.113 g/cm³ (99.26%), 17.303 g/cm³ (100.36%) and 17.288 g/cm³ (100.28%), respectively.

When sintering in the graphite press forms, the surfaces of the samples, the surfaces of the samples actively interact with carbon (see [28,38]). In order to analyze influence of carbonization to the characteristics of the alloys, the sintered samples were longitudinally cut, and then each of the surfaces was mechanically polished, which was followed by investigating the phase composition, the microstructure and microhardness of the surface and central layers of the  $W+10\,\%$ Ni samples.

The X-ray investigation results shown that the surface layers of all the samples, irrespective of the powder annealing mode, contain the phases W, Ni, WO2 as well as the  $\eta_1$ -phase Ni<sub>3</sub>W<sub>3</sub>C (PDF  $N_2$  01-078-5006, ICSD № 166814), which is generated when the oxidized W@Ni powders interact with the graphite press form. Formation of the impurity phases of the Wi-W-C system has also been previously detected during EPPS of the mechanically activated Ni-W nano-powders [41]. The reduced sintering temperatures could avoid intense formation of the carbide phases M<sub>12</sub>C and M<sub>6</sub>C that are often found in the tungsten pseudoalloys manufactured by EPPS at the temperatures above 1150 °C-1200 °C [42]. The diffraction patterns of the central layers (Fig. 4) of all the samples have exhibited the phases W, Ni and WO<sub>2</sub> that are contained in the initial powders. Let us note that the intensities of the peaks WO<sub>2</sub> in the sintered powders exceed the intensities of the peaks WO<sub>2</sub> in the W@Ni powders, thereby indicating oxidation of the W@Ni powders during EPPS.

The pseudoalloys have a homogenous microstructure and there are not traces of anomalous growth of grains or formation of the large particles of the  $\gamma$ -phase (Fig. 5). The thickness of the W/Ni interphase boundaries is very small, while their portion in the sintered tungsten pseudoalloys can be up to 0.81-0.90, 0.82-0.88 and 0.76-0.86 in the samples manufactured from the powders annealed at 400 °C, 500 °C and 600 °C, respectively. A portion of the interphase boundaries (bondability coefficient) has been calculated by analyzing the SEM images using the GoodGrains software as per the formula  $C_{SS} = 2N_{WW}/(2N_{WW} + N_{WNi})$ , where  $N_{WW}$  and  $N_{WNi}$  — the number of the W/W grain boundaries and the W/Ni interphase boundaries on the thinsection surface. The thin-section surface contains single pores of the submicron size, which are shown on Fig. 5 by the dashed line. The tungsten alloy sintered without isothermal holding from the powders annealed at 400 °C has an average grain size  $\sim 1-1.5 \,\mu\text{m}$ , while the nickel-based  $\gamma$ -phase is uniformly distributed along the grain boundaries of the tungsten pseudoalloy. It is clear from Fig. 5 that the increase of the temperature  $T_{\rm H2}$  and increase of the isothermal annealing time results in insignificant increase of the tungsten average grain size to  $1.5-2 \mu m$ .

Fig. 6 shows the results of investigations of hardness of the central layers of the samples of the tungsten pseudoalloys. It is clear from Fig. 6 that with increase of the time of isothermal holding there is reduction of pseudoalloys hardness due to grain growth (Fig. 5). Increase of the temperature of annealing the powders in hydrogen results in insignificant reduction of hardness which, in our opinion, is due reduction of the volume portion of oxides in the tungsten pseudoalloys. The maximum values of hardness are observed in the samples produced by EPPS from the submicron W@Ni powders annealed at  $400^{\circ}$ : in case of sintering without isothermal holding the HV hardness is  $(5.9 \pm 0.1)$  GPa,

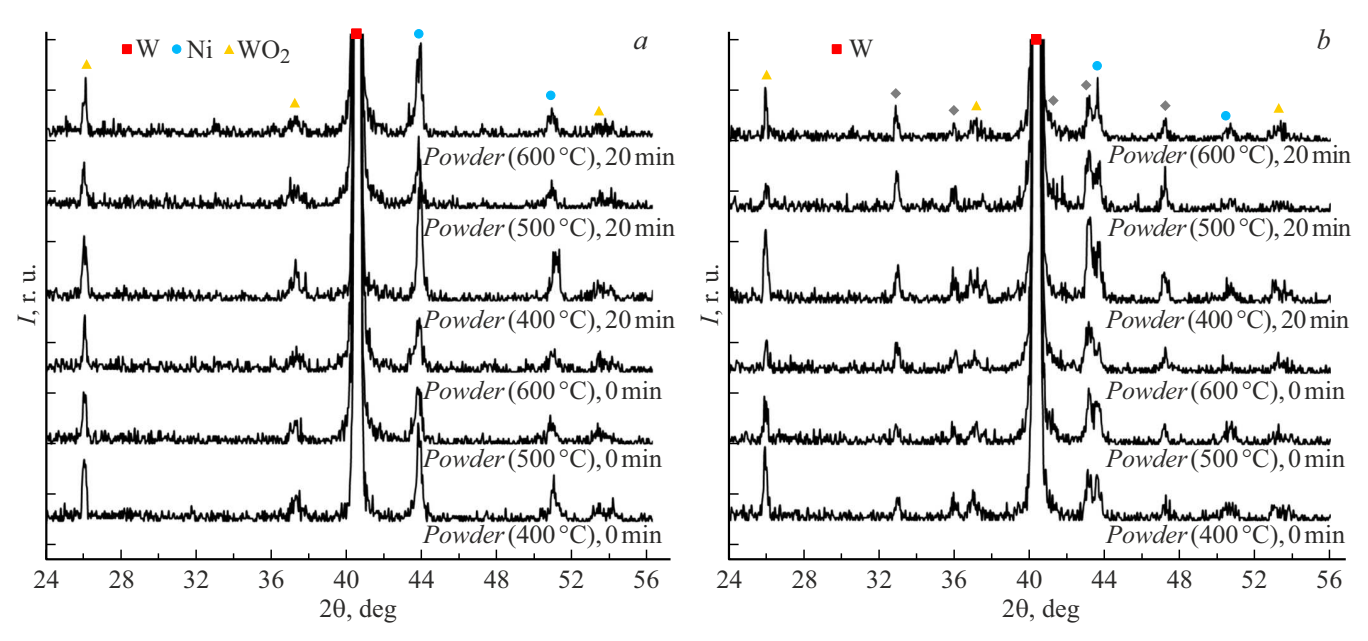


**Figure 4.** Diffraction patterns of the central (a) and surface (b) areas of the samples of the W + 10 %Ni pseudoalloys sintered from the powders annealed at the various temperatures  $(400 \,^{\circ}\text{C}, 500 \,^{\circ}\text{C}, 600 \,^{\circ}\text{C})$ . The time of isothermal holding  $(0, 20 \,\text{min})$  is specified on the diffraction patterns.

so is HV =  $(5.1\pm0.1)$  GPa with the 20-minute isothermal holding. During hardness measurement (with loading of  $10\,\mathrm{kg}$ ) there is severe plastic deformation of the surface without cracking (Fig. 6, b). It indicates increased fracture toughness when indenting the tungsten pseudoalloys.

Hardness of the produced W + 10 %Ni samples exceeds in 1.5 times hardness of the industrial coarse-grained W-Ni-Fe pseudoalloys [1-5] and by  $\sim 1\,\mathrm{GPa}$  exceeds the hardness of the W + 5%Ni pseudoalloy with the grain size of  $1.8 \,\mu\text{m}$ , which is produced by EPPS of the mechanically activated powders [29]. The dependences of hardness on the grain size in the coordinates  $HV - d^{-1/2}$ for the pseudoalloys W + 5%Ni [29] and W + 10%Niare compared in Fig. 7. The comparable values of hardness  $(5.8\,\text{GPa})$  in the  $W+5\,\%\text{Ni}$  pseudoalloy are provided only after mechanical activation of duration of at least 5 min, thereby resulting in intense pollution of the produced nano-powders by grinding products and formation of unwanted phases Fe<sub>6</sub>W<sub>6</sub>C, Ni<sub>2</sub>W<sub>4</sub>C, Ni<sub>4</sub>W and Ni<sub>17</sub>W<sub>3</sub> during EPPS. Mechanical activation of duration of 20 min has resulted in increase of hardness of the W + 5 %Nipseudoalloy to 7.6 GPa and reduction of the grain size to  $0.3 \,\mu m$  [29]. Brittleness and low hardness of the generated phases resulted in total reduction of hardness of the pseudoalloy with 5%Ni in comparison with the W + 10 %Ni pseudoalloy with the same grain size (Fig. 7). It is important to note that in the W + 10%Ni pseudoalloy all indenter imprints have a regular form and there is plastic deformation of the material without formation of microcracks (Fig. 6, b). The obtained result indirectly indicates that the tungsten  $W + 10 \,\% Ni$  pseudoalloys sintered from the W@Ni particles are characterized by good plasticity (in comparison with the fine-grained tungsten  $W+5\,\%$ Ni pseudoalloys, in which there is formation of radial cracks during hardness measurement [29]). In our opinion, the increased plasticity of the W@Ni pseudoalloys is caused by the high volume portion of the W/Ni interphase boundaries.

It is interesting to note that the pseudoalloys W + 5%Ni [29] and W + 10%Ni obey the Hall-Petch relationship, but a slope of the dependence  $HV - d^{-1/2}$ for the samples with the additive of 10 %Ni turns out to be in  $\sim 1.5-1.6$  times higher than for the pseudoalloys with 5%Ni (Fig. 7). It is a quite unexpected result, since it is usually supposed that increase of content of the low-melting  $\gamma$ -phase results in increase of the portion of the plastic interphase boundaries "tungsten-nickel", which have a lower coefficient of grain boundary strengthening in comparison with the usual grain boundaries "tungsten-In our opinion, the increase of strength of the W/Ni interphase boundaries in the fine-grained W + 10 %Nipseudoalloy is mainly caused by their small thickness, thereby complicating a process of their plastic deformation. Nickel in the W + 10 % Ni pseudoalloy is distributed uniformly along the surface of the tungsten particles and does not form separate large particles in triple junctions of the grains as it is during sintering of the powder compositions produced by mixing. The average calculated thickness of the interphase boundaries in the W + 10 %Ni pseudoalloy is  $50-70 \,\mathrm{nm}$  (for the grains  $d=1-1.5 \,\mu\mathrm{m}$ ) and effective operation of the Franck-Read source (formation of loops of lattice dislocations) is difficult in such nano-layers.

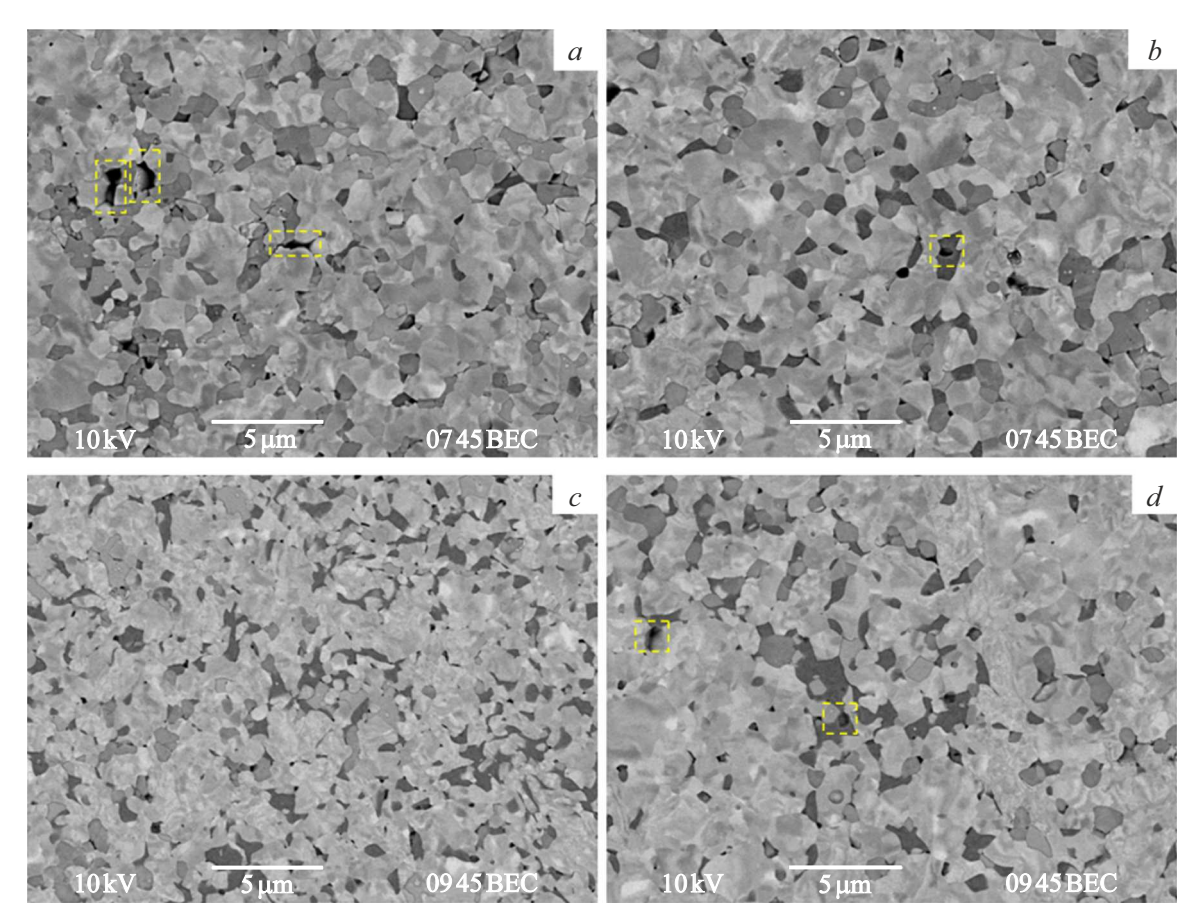


**Figure 5.** SEM images of the microstructure of the central layer of the samples of the W + 10 %Ni pseudoalloys sintered from the powders annealed at  $T_{\rm H2} = 400\,^{\circ}{\rm C}$  (a,b) and  $600\,^{\circ}{\rm C}$  (c,d). Sintering without isothermal holding (a,c) and with holding for 20 min (b,d).

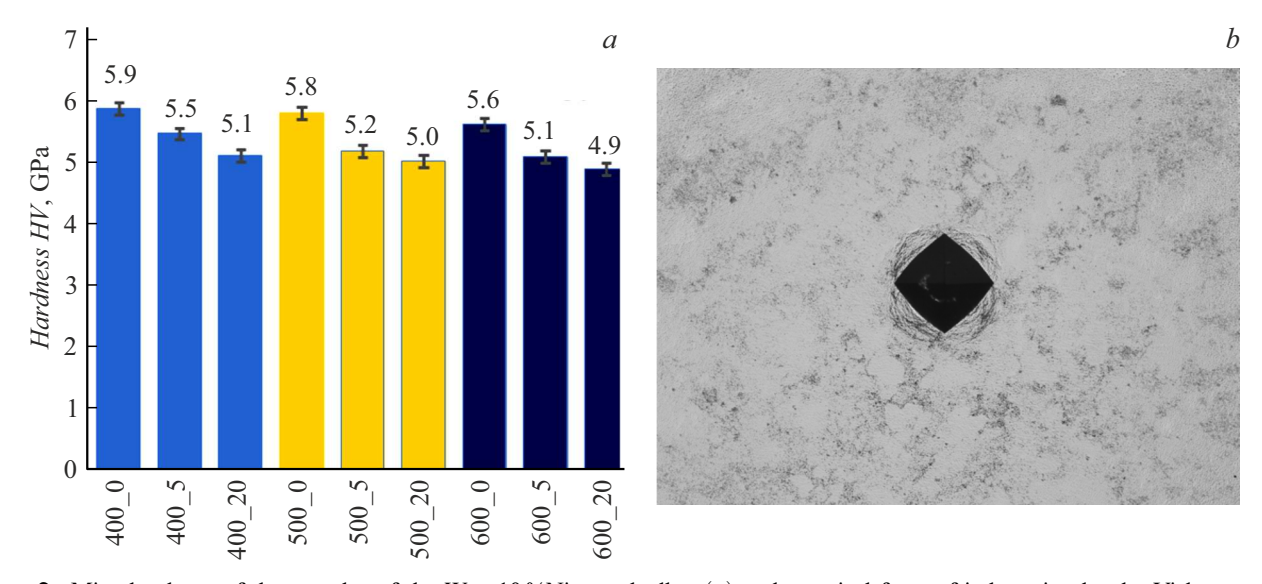


**Figure 6.** Microhardness of the samples of the W + 10 %Ni pseudoalloy (a) and a typical form of indentation by the Vickers pyramid on the sample surface (b). Designation of the sample in the "T-J" format: T— the temperature of annealing the W@Ni powder in hydrogen, [ $^{\circ}$ C], t— the time of isothermal holding, [min], at the sintering temperature (1050  $^{\circ}$ C).

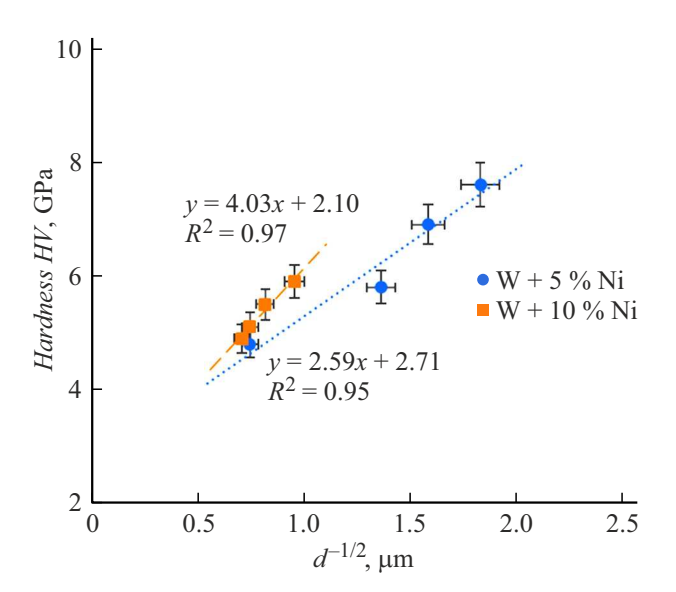


**Figure 7.** Dependence of hardness of the grain size for the pseudoalloys W + 5 % Ni [29] and W + 10 % Ni (herein).

# 3. Summary and analysis of the experimental results

Let us analyze mechanisms of electropulse sintering of the submicron W@Ni powders in conditions of high-rate heating and application of single-axis pressure.

As shown above, the dependence of shrinkage of the W@Ni powders on the heating temperature L(T) is of the three-stage nature (Fig. 3, a). The dependence L(T) can be characterized by an interval of "low" temperatures  $(T < T_1)$ , in which the shrinkage rate is low (the stage I), an interval of "average" temperatures  $T_1 < T < T_2$ , which corresponds to the state of intense shrinkage (the stage II), and, finally, an interval of "high" temperatures  $T > T_2$ , in which the powders shrinkage rate is reduced again [43].

Let us define diffusion mechanisms that control the process of compaction of the W@Ni powders at the stages II and III which define the density and the parameters of the UFG microstructure of the tungsten pseudoalloys.

The kinetics of compaction of the W@Ni powders within the "average" temperatures (the stage II) can be analyzed by using the model [44], which describes an initial stage of non-isothermal sintering of the particles in conditions of competition of processes of volume and grainboundary diffusion and plastic deformation as well. Positive experience of application of the Yang-Cutler model [44] for describing the kinetics of electropulse sintering of the tungsten pseudoalloys is given in the papers [25,29], so we will not describe this model and its assumptions in detail. Within the framework of the Yang-Cutler model, the effective energy of EPPS activation  $(mQ_{s2}, kT_m)$  can be determined by a slope of the dependence  $\ln(T\partial \varepsilon/\partial T) - T_m/T$ , where  $\varepsilon$  — relative shrinkage,  $T_m$  — the material melting temperature, while the value of the coefficient m depends on a dominant diffusion mechanism (m = 1/3) for the

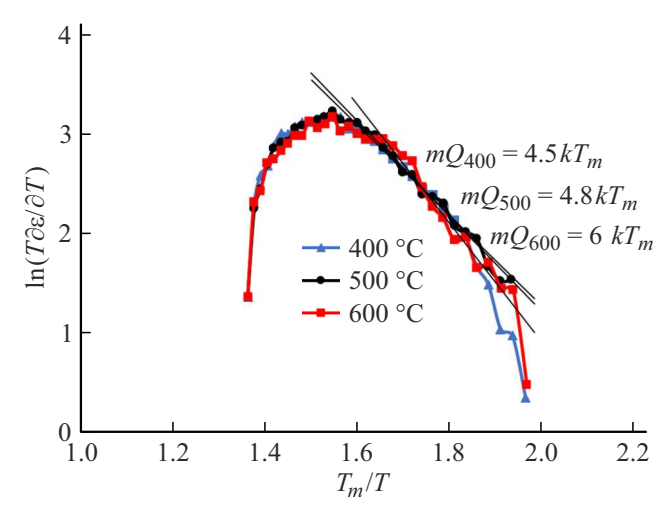


**Figure 8.** Temperature dependences of shrinkage of the W@Ni powders in the coordinates  $\ln(T\partial \varepsilon/\partial T) - T_m/T$ . Calculation of the sintering activation energy on the stage II using the Yang-Cutler model.

case of grain-boundary diffusion, m=1/2 for diffusion in the crystal lattice, m=1 for viscous flow (creep) of the material [44,45]). When determining EPPS activation energy, the melting temperature of the W + 10 weight% Ni pseudoalloy was assumed to be a Ni melting temperature. ( $T_m=1726\,\mathrm{K}$ ). It has been shown in [25,29] that for the tungsten pseudoalloys produced by mixing the submicron powders (W, Ni, Fe), m=1; and when sintering the mechanically activated nano-powders m=1/3.

The dependences  $\ln(T\partial \varepsilon/\partial T) - T_m/T$  of Fig. 8 are of a two-stage nature, which is typical for the case of nonstationary heating (see [25,29,44]).

It is clear from Fig. 8 that when m=1 the effective energy of activation of sintering of the W@Ni powders is close to the energy of activation of diffusion along the grain boundaries in nickel ( $\sim 8\,\mathrm{kT}_m = 115\,\mathrm{kJ/mol}$  [46]).The increase of temperature of pre-annealing of the W@Ni powders in hydrogen from  $400\,^{\circ}\mathrm{C}$  to  $600\,^{\circ}\mathrm{C}$  does not substantially affect the value of sintering activation energy at the stage II ( $Q_{s2}$ ). ( $mQ_{S2}\sim 5.8-6.4\,\mathrm{kT}_m$ ) The obtained result indicates that the key mechanism of compaction of the submicron W@Ni powders at the stage II is Coble creep (see also the review [47]).

The EPPS activation energy can be calculated within the "high" heating temperatures (the stage III) by using a model of diffusion dissolution of pores near grain boundaries of the fine-grained materials [48]. In this case, the sintering activation energy  $Q_{s3}$  is determined by the slope of the dependence  $\rho(T)/\rho_{th}$  in the coordinates  $\ln(\ln(\alpha \cdot \rho/\rho_{th}/(1-\rho/\rho_{th})) - T_m/T$ , where  $\alpha = 0.33$ —the coefficient of compaction of compacts of the W@Ni powders (Fig. 9). The average accuracy of determining the value  $Q_{s3}$  is  $\pm 0.5 \, \mathrm{kT}_m$ .

The dependences  $\ln(\ln(\alpha \cdot \rho/\rho_{th}/(\rho/\rho_{th}-1)) - T_m/T$  for the W@Ni powders at the stage III are of a usual linear

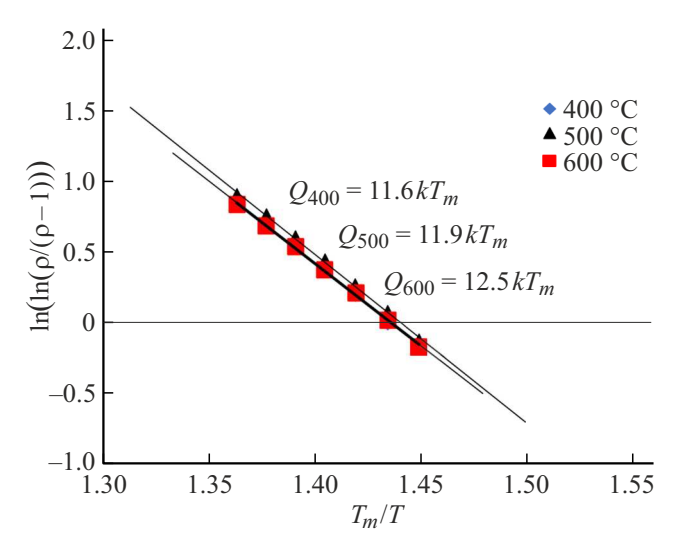


**Figure 9.** Temperature dependences of compaction in the coordinates  $\ln(\ln(\alpha \cdot \rho/\rho_{th}/(1-\rho/\rho_{th})) - T_m/T$  for the W@Ni powders. Calculation of the sintering activation energy at the stage III.

nature. The temperature of pre-annealing does not affect the sintering activation energy  $Q_{s3}$ , which is  $\sim 11.5-12.2\,\mathrm{kT}_m$ . The sintering activation energy at the stage III exceeds the energy of activation of grain-boundary diffusion in nickel, which is probably related to presence of the Ni<sub>4</sub>W particles in the powders, which during heating are transformed into the particles of the  $\eta_1$ -phase Ni<sub>3</sub>W<sub>3</sub>C. Let us note that release of the Ni<sub>4</sub>W particles results in strengthening of the nickel alloys [49,50], while stress of flow of the nickel alloys with the Ni<sub>4</sub>W particles at the temperatures above 1000 °C is very high [51] and is much greater than the stress (70 MPa), at which there is electropulse sintering of the tungsten W + 10 %Ni pseudoalloy. Besides, when the heating temperature is increased, the particles of the phase Ni<sub>4</sub>W grow due to absorption of the Ni plastic phase [52]. It results in reduction of the content of the Ni viscous metal phase inside the tungsten W + 10 % Ni pseudoalloy and, as a consequence, in reduction of the powder compaction rate.

Thus, it can be concluded that the grain-boundary diffusion processes control intensity of high-rate electropulse sintering of the W@Ni powders at the stage III.

#### **Conclusions**

1. The joint application of the method of chemical metallurgy deposition of thin nickel layers to the surface of submicron tungsten particles and the method of their high-rate electropulse sintering makes it possible to produce the highly-dense fine-grained tungsten W+10 weight%Ni pseudoalloys. Due to optimization of the modes of preannealing of the W@Ni powders in hydrogen, there is reduction of the number of particles of the oxides  $WO_2$  in the tungsten alloys and, as a consequence, increase of the grain size. The samples of the fine-grained tungsten

pseudoalloys have higher hardness and viscosity when indenting due to a high volume portion of the W/Ni interphase boundaries and small extension thereof.

2. The Yang-Cutler model and the model of diffusion dissolution of the pores near the grain boundaries have been taken to determine the energy of activation of high-rate sintering of the W@Ni powders. It is shown that the energy of activation of sintering of the W@Ni powders at the intense shrinkage stage is close to the energy of activation of grain-boundary diffusion and weakly depends on the time of pre-annealing of the powders in hydrogen. The higher energies of activation at the high-temperature sintering stage are caused by presence of the Ni<sub>4</sub>W particles, which complicate the process of plastic flow of nickel.

### **Funding**

This study was supported by grant from the Russian Science Foundation  $N_2$  22-79-10080.

#### Conflict of interest

The authors declare that they have no conflict of interest.

### References

- J.V. Haag IV, J. Wang, D.J. Edwards, W. Setyawan, M. Murayama. Scr. Mater., 213, 114587 (2022).
  DOI: 10.1016/j.scriptamat.2022.114587
- [2] J. Das, G.A. Rao, S.K. Pabi. Mater. Sci. Eng. A, 527, 7841 (2010). DOI: 10.1016/j.msea.2010.08.071
- [3] K.V. Povarova, P.V. Makarov, A.D. Ratner, E.K. Zavarzina, K.V. Volkov. Metally, 4, 39 (2002) (in Russian).
- [4] Y. Sahin. J. Powder Technol., 3-4, 1 (2014). DOI: 10.1155/2014/764306
- [5] A. Kumari, M. Sankaranarayana, T.K. Nandy. Int. J. Refr. Met. Hard Alloys, 67, 18 (2017).
   DOI: 10.1016/j.ijrmhm.2017.05.002
- [6] R.M. German. Int. J. Refr. Met. Hard Alloys, 108, 105940 (2022). DOI: 10.1016/j.ijrmhm.2022.105940
- [7] X. Gong, J.L. Fan, F. Ding, M. Song, B.Y. Huang,
  J.M. Tian. Mater. Sci. Eng. A, 528, 3646 (2011).
  DOI: 10.1016/j.msea.2011.01.070
- [8] S.H. Islam, X. Qu, S.J. Askari, M. Tufail, X. He. Rare Metals, 26, 200 (2007). DOI: 10.1016/S1001-0521(07)60201-0
- [9] L. Zhang, B. Chen, X. Chen, J. Sun, Y. Huang,
  W. Liu, Y. Ma. Mater. Sci. Eng. A, 852, 143696 (2022).
  DOI: 10.1016/j.msea.2022.143696
- [10] R. Gero, L. Borukhin, I. Pikus. Mater. Sci. Eng. A, 302, 162 (2001). DOI: 10.1016/S0921-5093(00)01369-1
- [11] E. Lang, A. Kapat, T.W. Morgan, J.P. Allain. J. Nucl. Mater., 544, 152672 (2021). DOI: 10.1016/j.jnucmat.2020.152672
- [12] L.A. El-Guebaly, W. Setyawan, C.H. Henager Jr., R.J. Kurtz, G.R. Odette. Nucl. Mater. Energy., 29, 101092 (2021). DOI: 10.1016/j.nme.2021.101092
- [13] R. Neu, H. Maier, M. Balden, S. Elgeti, H. Gietl, H. Greuner, A. Herrmann, A. Houben, V. Rohde, B. Sieglin, I. Zammuto. Fusion Eng. Des., 124, 450 (2017). DOI: 10.1016/j.fusengdes.2017.01.043

- [14] S. Tõkke, T. Laas, J. Priimets, V. Mikli, M. Antonov. Fusion Eng. Des., 164, 112215 (2021).
   DOI: 10.1016/j.fusengdes.2020.112215
- [15] H. Maier, R. Neu, T. Schwarz-Selinger, U. von Toussaint, A. Manhard, T. Dürbeck, K. Hunger. Nucl. Fusion, 60(12), 126044 (2020). DOI: 10.1088/1741-4326/abb890
- [16] G. Parabhu, N.A. Kumar, M. Sankaranarayana, T.K. Nandy. Mater. Sci. Eng. A, 607, 63 (2014). DOI: 10.1016/j.msea.2014.03.130
- [17] V.N. Chuvil'deev, A.V. Nokhrin, G.V. Baranov, M.S. Boldin, A.V. Moskvicheva, N.V. Sakharov, D.N. Kotkov, Yu.G. Lopatin, V.Yu. Belov, Yu.V. Blagoveshchenskii, N.A. Kozlova, D.A. Konychev, N.V. Isaeva. Metally, 2, 51 (2014) (in Russian).
- [18] Y.J. Wu, Y.K. Li, D.H. Yu. Mater. Sci. Forum., **849**, 745 (2016).
- [19] Z.B. Li, K. He, G.H. Zhang, K.C. Chou. Metall. Mater. Trans. A, 51, 3090 (2020). DOI: 10.1007/s11661-020-05761-w
- [20] D.V. Edmonds. Int. J. Refract. Met. Hard Mater., **10**, 15 (1991). DOI: 10.1016/0263-4368(91)90007-B
- [21] P.V. Krasovskii, A.V. Samokhin, A.A. Fadeev, M.A. Sinayskiy, S.K. Sigalev. J. Alloys Compd., 250, 265 (2018). DOI: 10.1016/j.jallcom.2018.03.367
- [22] N. Deng, J. Li, W. Wang, D. Qu, K. Zhang, Z. Zhou. Int. J. Refract. Met. Hard Mater., 95, 105447 (2021). DOI: 10.1016/j.ijrmhm.2020.105447
- [23] N. Deng, J. Li, S. Liang, H. Sun, Y. Guo. Powder Tech., 407, 117632 (2022). DOI: 10.1016/j.powtec.2022.117632
- [24] L. Ding, D.P. Xiang, Y.Y. Li., C. Li, J.B. Li. Int. J. Refract. Met. Hard Mater., 33, 65 (2012). DOI: 10.1016/j.ijrmhm.2012.02.017
- [25] A.V. Nokhrin, N.V. Malekhonova, V.N. Chuvil'deev, N.V. Melekhin, A.M. Bragov, A.R. Fillipov, M.S. Boldin, E.A. Lansev, N.V. Sakharov. Metals, 13, 1432 (2023). DOI: 10.3390/met13081432
- [26] S. Eroglu, T. Baykara. J. Mater. Process. Tech., 103, 288 (2000). DOI: 10.1016/S0924-0136(00)00499-4
- [27] M. Tokita. Ceramics, **4**, 160 (2021). DOI: 10.3390/ceramics4020014
- [28] E. Olevsky, D. Dudina. Field-Assisted Sintering (Springer Int. Publ., 2018), DOI: 10.1007/978-3-319-76032-2
- [29] E.A. Lantsev, N.V. Malekhonova, A.V. Nokhrin, K.E. Smetanina, A.A. Murashov, G.V. Shcherbak, A.V. Voronin, A.A. Atopshev. ZhTF, 93, (in Russian). 1550 (2023). DOI: 10.61011/JTF.2023.11.56486.143-23
- [30] E.A. Lantsev, N.V. Malekhonova, V.N. Chuvil'deev, A.V. Nokhrin, Yu.V. Tsvetkov, Yu.V. Blagoveshchenskii, M.S. Boldin, P.V. Andreev, K.E. Smetanina, N.V. Isaeva. FKhOM, 1, 24 (2022) (in Russian). DOI: 10.30791/0015-3214-2022-2-35-54
- [31] E.A. Lantsev, N.V. Malekhonova, V.N. Chuvil'deev, A.V. Nokhrin, Yu.V. Tsvetkov, Yu.V. Blagoveshchenskii, M.S. Boldin, P.V. Andreev, K.E. Smetanina, N.V. Isaeva. FKhoM, 2, 35 (2022) (in Russian). DOI: 10.30791/0015-3214-2022-2-35-54
- [32] D.V. Dudina, N.Yu. Cherkasova. Mater. Lett., **365**, 136411 (2024). DOI: 10.1016/j.matlet.2024.136411
- [33] M.B. Shongwe, S. Diouf, M.O. Durowoju, P.A. Olubambi, M.M. Ramakokovhu, B.A. Obadele. Int. J. Refract. Met. Hard Mater., 55, 16 (2016). DOI: 10.1016/j.ijrmhm.2015.11.001

- [34] A.A. Mazilkin, B.B. Straumal, S.G. Protasova, M.F. Bulatov,
  B. Baretzky. Mater. Lett., 192,101 (2017).
  DOI: 10.1016/j.matlet.2016.12.049
- [35] B. Guennec, D. Tingaud, R. Pires-Brazuna, L. Perrière,
  N. Horikawa, G. Dirras. J. Alloy. Compd., 966,
  171490 (2023). DOI: 10.1016/j.jallcom.2023.171490
- [36] Z.Z. Fang, C. Ren, M. Simmons, P. Sun. Int. J. Refract. Met. Hard Mater., 92, 105281 (2020). DOI: 10.1016/j.ijrmhm.2020.105281
- [37] D.V. Dudina, B.B. Bokhonov. Adv. Powd. Tech., 28, 641 (2017). DOI: 10.1016/j.apt.2016.12.001
- [38] K.E. Smetanina, P.V. Andreev, A.V. Nokhrin, E.A. Lantsev, V.N. Chuvildeev. J. Alloy. Compd., 973, 172823 (2024). DOI: 10.1016/j.jallcom.2023.172823
- [39] E. Fortuna, K. Sikorski, K.J. Kurzydlowski. Mater. Charact., 52, 323 (2004). DOI: 10.1016/j.matchar.2004.06.011
- [40] D.P. Rodionov, I.V. Geras'eva, Yu.V. Khlebnikova, V.A. Sazonova, B.K. Sokolov. FMM, 99, 88 (2005) (in Russian).
- [41] D.V. Dudina, B.B. Bokhonov, A.V. Ukhina, A.G. Anisimov, V.I. Mali, M.A. Esikov, I.S. Batraev, O.O. Kuzhnechik, L.P. Pilinevich. Mater. Lett., 168, 62 (2016). DOI: 10.1016/j.matlet.2016.01.018
- [42] J. Wang, J. Ding, W. Liu, Y. Ma, W. Zhu, S. Meng, C. Liang, Q. Cai. Int. J. Refract. Met. Hard Mater., 114, 106251 (2023). DOI: 10.1016/j.ijrmhm.2023.106251
- [43] M.N. Rahaman. Ceramic processing and sintering. 2nd ed. (Marcel Dekker Inc., NY., 2003)
- [44] W.S. Young, I.B. Culter. J. Am. Ceram. Soc., 53, 659 (1970). DOI: 10.1111/j.1151-2916.1970.tb12036.x
- [45] A.K. Nanda Kumar, M. Watabe, K. Kurokawa. Ceram. Int., 37, 2643 (2011). DOI: 10.1016/j.ceramint.2011.04.011
- [46] G.Dzh. Frost, M.F. Eshbi. *Karty mekhnizmov deformatsii* (Metallurgiya, Chelyabinsk, 1989) (in Russian).
- [47] J. Webb, S. Gollapudi, I. Charit. Int. J. Refract. Met. Hard Mater., 82, 69 (2019). DOI: 10.1016/j.ijrmhm.2019.03.022
- [48] V.N. Chuvil'deev, M.S. Boldin, Ya.G. Dyatlova, V.I. Rumyant-sev, S.S. Ordan'yan. Neogranicheskie materialy, 51, 1128 (2015) In Russian). DOI: 10.7868/S0002337X15090031
- [49] Y. Li, Y. Xiong, H. Li, S. Han, F. Ren, C. Wang. Coatings, 14, 230 (2024). DOI: 10.3390/coatings14020230
- [50] S. Hayata, S. Oue, H. Nakano, T. Takahashi. ISIJ Int., 55, 1083 (2015). DOI: 10.2355/isijinternational.55.1083
- [51] Y. Li, Y. Xiong, J. Tang, S. Han, F. Ren, C. Wang, S. Wang. Coatings, 14, 323 (2024). DOI: 10.3390/coatings14030323
- [52] S. Inomata, M. Kajihara. J. Alloy. Comp., 509, 4958 (2011).
  DOI: 10.1016/j.jallcom.2011.01.139

Translated by M.Shevelev